Calibration of Two Qutrit Cross-Resonance for Excited States of Superconducting Qubits

Sunil Vittal, Nataliia Khotaintseva*

May 2024

Abstract

We attempt to generalize protocols for calibrating a two-qubit Cross-Resonance (CR) entangling gate on the $|0\rangle, |1\rangle$ states to the $|1\rangle, |2\rangle$ states. The typical pulse-level description for the CR gate involves Gaussian Square pulses on control channels between the qubits with cancellation tones on the target qubit. We mimic this pulse sequence by driving the control qubit at the $|1\rangle \rightarrow |2\rangle$ transition frequency to generate a rotation on the target qubit. Unfortunately, we run into large difficulties in the calibration process, evidenced by the large deviation from theoretical expectations within Hamiltonian Tomography experiments and lack of predictable behavior as pulse durations increase. While we report results for these kinds of experiments for completion, the results are not indicative of proper calibration, likely due to internal hardware protection against qubits staying within higher energy states in control channels. Nonetheless, we calibrate the amplitude and phase of the CR tones on the control channel for our gate and acquire state fidelities of $82.035\%, 64.589\%, 70.86\%, 65.64\%$ for the $|11\rangle, |12\rangle, |21\rangle, |22\rangle$ states respectively via Quantum State Tomography.

Introduction

Transmon computers feature superconducting qubits, incorporating a quantum harmonic oscillator with energy levels separated by different transition frequencies. While this is just a hardware specification, in traditional quantum computation with the $|0\rangle$ and $|1\rangle$ qubit computational basis, one runs into *leakage errors*, which are errors involving qubits that become overexcited, in the sense that they leak into higher energy levels. These are particularly important since the leakage of quantum information from the computational basis causes correlated errors on neighboring qubits through multi-qubit interactions. As a result, a major focus of quantum error correction is pursuing correction of leakage errors. [1]

*While she is technically a part of my lab group, she did not contribute anything to this project. All coding, experiments, report writing, and proposal writing were completed by myself (Sunil), and it seems as if she made no effort to learn the background for this project to run experiments independently or understand what is being done experimentally. Her only contribution was giving me her email to run experiments with on the IMBQ platform. I would appreciate if the handling of this project alone was factored into the review of this submission. Hope you enjoy reading!

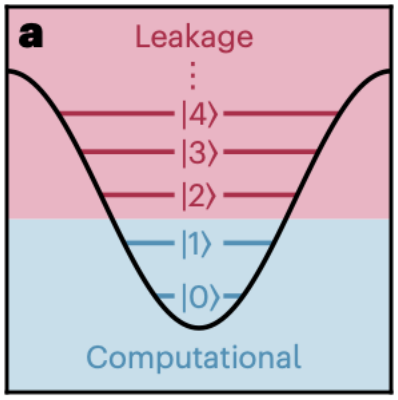

Figure 1: Taken from [1]. Illustration of energy levels in superconducting qubits.

While leakage errors present huge issues in quantum computation, there have been some results utilizing qutrits to construct quantum logical gates. For instance, [2] implements the Toffoli/CCNOT gate by utilizing a $|2\rangle-$controlled not gate, among other ternary logic gates. In particular, by utilizing a control *qutrit*, the authors are able to simplify the gate decomposition of the Toffoli gate. While their implementation of the gate results involves utilizing $|2\rangle$ to invert the target qubit, we desire to explore quantum computation within the ternary logic world by focusing on the two dimensional Hilbert space $\mathcal{H}_{12}$ generated by $\{|1\rangle, |2\rangle\}$. With this thinking we isolate a qubit within the less stable $|1\rangle, |2\rangle$ basis states world rather than the relatively stable $|0\rangle, |1\rangle$ basis states.

When typically considering qudits, one defines Pauli gates via

$$X|j\rangle = |j+1 \bmod d\rangle \quad \text{and} \quad Z|j\rangle = \omega^j|j\rangle$$

for $\omega = e^{2\pi i/d}$. We can use these two gates to define more gates via $E_{r,s} = X^r Z^s$ for $0 \leq r, s \leq d-1$. Since we're isolating the $|1\rangle, |2\rangle$ states in $d = 3$, it doesn't make sense to follow this implementation and we simply generalize the operators to fix the $|0\rangle$ state but perform the analogous operation on the $|1\rangle, |2\rangle$ states. As a result, our Pauli Operators become

$$X = \begin{pmatrix} 1 & 0 & 0 \\ 0 & 0 & 1 \\ 0 & 1 & 0 \end{pmatrix} \qquad Z = \begin{pmatrix} 1 & 0 & 0 \\ 0 & 1 & 0 \\ 0 & 0 & -1 \end{pmatrix} \qquad Y = iXZ = \begin{pmatrix} 1 & 0 & 0 \\ 0 & 0 & -i \\ 0 & i & 0 \end{pmatrix} \tag{0.1}$$

Note that this is simply a 3×3 block matrix where $|0\rangle \to |0\rangle$ and all operations are done on $|1\rangle, |2\rangle$. [3].

With this context aside, in this report, we attempt to calibrate a Cross-Resonance (CR) gate designed for the $|1\rangle, |2\rangle$ states using the IBM Quantum Platform service, which gives access to quantum computers for users to run experiments on. The CR gate is an entangling gate between

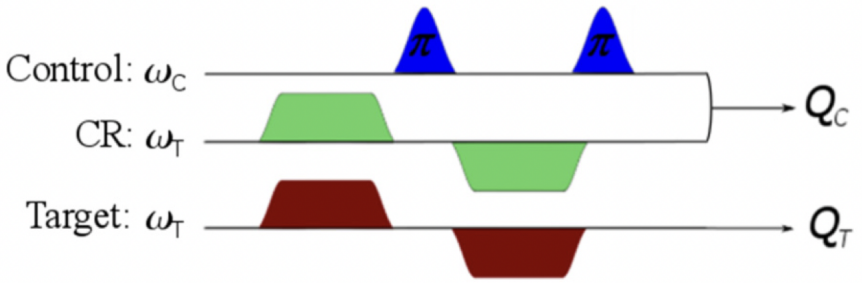

Figure 2: Pulse Schematic for an Echoed CR Gate where the control qubit is driven at the frequency of the target qubit due to CR pulses on the control channel connecting the two qubits. There is also cancellation rotations on the target qubit to further increase gate fidelity.

a control qubit $|\psi\rangle$ and target qubit $|\phi\rangle$. The gate is physically implemented by driving $|\psi\rangle$ at the frequency of $|\phi\rangle$ to cause a $Z \otimes X$ evolution on the system. The CR gate can be approximated by a unitary evolution

$$U_{CR} \approx e^{-it_{CR}H_{CR}} \tag{0.2}$$

where H_{CR} is a time-independent hamiltonian described by

$$H_{CR} = \omega_{ZI}ZI + \omega_{ZX}ZX + \omega_{ZY}ZY + \omega_{ZZ}ZZ + \omega_{IX}IX + \omega_{IY}IY + \omega_{IY}IY \tag{0.3}$$

where the $\otimes$ are omitted for readability. One notices that to effectively implement U_{CR} as a ZX rotation, one desires the ZX term of the above Hamiltonian to be isolated. In fact, it's been shown $U_{ZX} = e^{-i\frac{\theta_{ZX}}{2}ZX}$ can generate a maximally entangling state from a pure state, meaning if one can isolate the ZX term of the hamiltonian and generate a $\pi/2$ rotation, the CR gate is locally equivalent to a CNOT gate. Nonetheless, the lingering terms in H_{CR} lead to coherent errors between the qubits, so we desire to suppress these terms as much as possible throughout our calibration. [4]

While suppressing unwanted interactions is a goal during calibration, there are many more difficulties to consider within this experiment. The $|2\rangle$ state is much more unstable than the $|1\rangle$, so decoherence occurs more often and at much larger proportions when working in $\mathcal{H}_{12}$. Moreover, as a principle, since the point of a good quantum computer is to prevent states from being in leaked states, there could be architectural blocks causing CR pulses with high energy levels from not functioning properly. Fighting against these error correcting protocols could lead to other errors on our qubits.

As a result, the I hypothesize that dynamics for a CR gate between $|1\rangle$ and $|2\rangle$ incorporate decoherence of the control qubit over time as gate lengths increase and thus a 'calibrated' CR gate for this pair of energy levels cannot reach the fidelities of a standard CR gate. Moreover, decoherence of the control qubit overtime not only results from detuning, but rather could result from error correction protocols within the system. While I have no way of testing this, we can still

see what happens to the control qubit throughout the attempted calibration process.

Due to these anticipated and unavoidable issues, I expect to state fidelity for the two qubit computational basis $\{|11\rangle, |12\rangle, |21\rangle, |22\rangle\}$ states to be around 70% when we run *Quantum State Tomography* with the 'calibrated' gate. The inability for this experiment to function close to theoretical expectations is likely due to (relatively) low CNOT errors on IBM's quantum computers. Moreover, the larger the separation between energy levels, the more difficult this experiment likely is, yet a larger seperation of energy levels is needed to classify data properly to prevent measurement errors. Essentially, we have a tradeoff of errors that may or may not jeopordize the results of this experiment since we're essentially performing cross resonance when our control qubit is leaked.

1 Experimental Design and Results

All experiments below were done on qubits $0, 1$ in the IBM Brisbane computer. Since there are no available gates for the $|2\rangle$ state, we must first define basic Pauli Operators. Much like the $|0\rangle, |1\rangle$ case, this involves finding the transition frequency between $|1\rangle$ and $|2\rangle$. We utilize these transition frequencies to calibrate X gates for each qubit (While this is really a qutrit, I will use the term qubit throughout the rest of the paper to mean a transmon that is either $|1\rangle$ or $|2\rangle$. I'll use the term qutrit when the $|0\rangle$ is involved in the experiment).

After calibrating generalized X gates, we form a measurement classifier to classically measure our qutrits as one of $|0\rangle, |1\rangle, |2\rangle$. From these basic objects defined, we begin calibrating our CR gate via a series of hamiltonian tomography experiments which will be explained in a dedicated section on the CR calibration process. For fits regarding transition frequencies and π-pulse amplitudes, we refer the reader to the appendix.

1.1 CR Gate Calibration

IBMs backend CR gate implementation follows the below pulse schedule. One notices that this is an echoed CR implementation with cancellation tones on the target qubit. Per the implementation in [5] and [4], the calibration of this gate should take four experiments. In particular, to calculate the amplitude of the tones on the control channel, we initialize our state in $|11\rangle$ and perform an amplitude sweep of the gate and analyze the expectation value $\langle Z\rangle$ by calculating $P(1) - P(2)$. We look for the value such that $\langle Z\rangle = 0$ since this represents a uniform superposition of the $|1\rangle$ and $|2\rangle$ states.

Note that another implementation of the CR gate in [4] illustrates only a single cross resonance tone on the control channel, but the callibration of such a gate doesn't allow us to do the above amplitude callibration since the time independent hamiltonian has nonneglible non ZX interaction terms. As [4] states, the time independent hamiltonian for the echoed CR gate is the following

$$H_{CR} =\simeq \Omega(A, \phi)(\cos\phi_0 ZX + \sin\phi_0 ZY) + \varepsilon$$

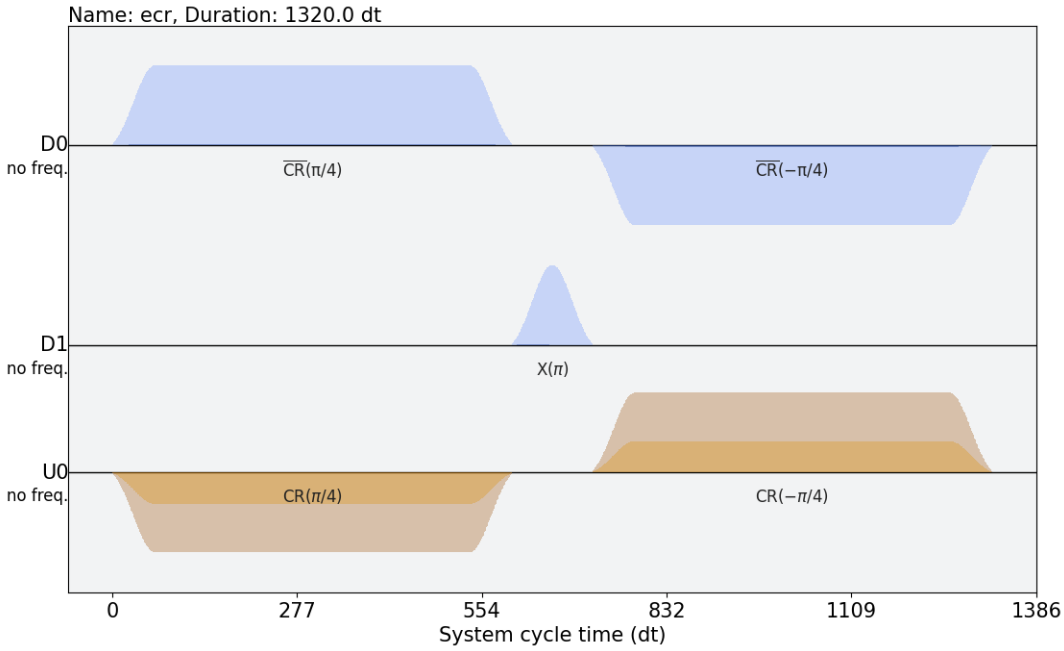

Figure 3: IBM Sherbrooke's implementation of the Cross Resonance gate on $|0\rangle$ and $|1\rangle$ states with CR pulses on the Control Channel and Cancellation Rotations on the Target Qubit.

where Ω is the drive strength of the pulses, ϕ is the phase of the pulse, and ε neglible, but nonzero other interaction terms of the hamiltonian that aren't eliminated by the echo sequence. Since the time-independent hamiltonian indicates that the ZX and ZY terms are much larger than other interaction terms, we find that $\langle Z\rangle \approx \cos(\theta)$, which holds true for the ideal version of this gate.[5]

Utilizing this amplitude, we perform a *Hamiltonian Tomography* Experiment on the CR gates where we perform the CR pulse on the control channel and measure the target qubit in the X, Y, Z bases. We then plot these values and fit them to measure the interaction rates ω_{ij} in (0.3). To get into the details of the Hamiltonian Tomography for the CR gate, we refer to the exposition from [6] in the appendix (The mathematical derivations are taken from [6] and much of the wording is unchanged, hence the quotes). Long story short: The fit functions[1] are

$$\langle \hat{X}(t)\rangle_n = \frac{1}{\Omega^2}\left(-\Delta\Omega_x + \Delta\Omega_x \cos(\Omega t) + \Omega\Omega_y \sin(\Omega t)\right)$$

$$\langle \hat{Y}(t)\rangle_n = \frac{1}{\Omega^2}\left(\Delta\Omega_y - \Delta\Omega_y \cos(\Omega t) - \Omega\Omega_x \sin(\Omega t)\right)$$

$$\langle \hat{Z}(t)\rangle_n = \frac{1}{\Omega^2}\left(\Delta^2 + \left(\Omega_x^2 + \Omega_y^2\right)\cos(\Omega t)\right)$$

where $\Omega = \sqrt{\Delta^2 + \Omega_x^2 + \Omega_y^2}$ for each control qubit preparation n. The above fits provide the parameters Ω_x^i, Ω_y^i, and Δ^i for the control qubit prepared in states $i = |1\rangle, |2\rangle$. The interaction

[1] While the fit functions are theoretical functions with respect to the $|0\rangle$ and $|1\rangle$ case, we will see that the $|1\rangle$ and $|2\rangle$ case requires consideration of a damped oscillator and extra offset constants

rates ω_{ij} are

$$\omega_{IX} = \frac{1}{2}\left(\Omega_x^0 + \Omega_x^1\right) \qquad \omega_{ZX} = \frac{1}{2}\left(\Omega_x^0 - \Omega_x^1\right) \tag{1.1}$$

$$\omega_{IY} = \frac{1}{2}\left(\Omega_y^0 + \Omega_y^1\right) \qquad \omega_{ZY} = \frac{1}{2}\left(\Omega_y^0 - \Omega_y^1\right) \tag{1.2}$$

$$\omega_{IZ} = \frac{1}{2}\left(\Delta^0 + \Delta^1\right) \qquad \omega_{ZZ} = \frac{1}{2}\left(\Delta^0 - \Delta^1\right) \tag{1.3}$$

Using these fit functions, we need to perform 3 tomography experiments to theoretically maximize the fidelity of our gate. The first is to calibrate the phase of the tone on the control channel that minimizes ω_{ZY} and the phase of the cancellation tones on the target qubit that minimizes the ω_{IY} term. The second and third are to determine the amplitude of the cancellation tones on the target qubit.[5]

1.1.1 CR gate Amplitude

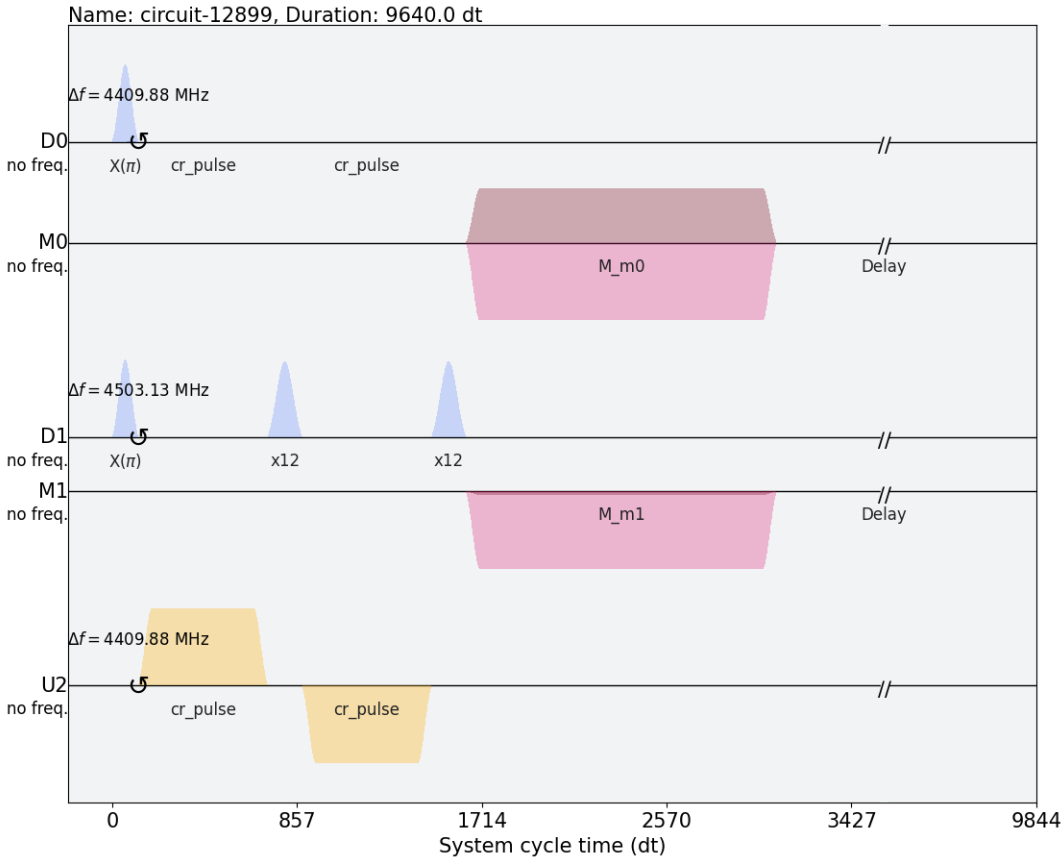

Figure 4: CR Amplitude Sweep Pulse Schdule

We take the default pulse duration and widths from the backend calibration of the IBM computer

which for a sampling time of $dt = 0.5ns$, the pulse duration is $600dt = 300ns$ and the width is $472dt = 236ns$. From sweeping the pulse amplitude, we can form an initial guess from the parameters of the IBM calibrated CR gate, which has control channel pulses of amplitude ≈ 0.17. We do our amplitude sweep with varied CR amplitudes from 0 to 0.3 in increments of 0.005 with an initial state $|11\rangle$. We average over 2048 shots per amplitude.

By setting the frequency on the control channel to the fitted $|1\rangle \rightarrow |2\rangle$ transition frequency of the target qubit, we drive the control qubit at this transition frequency. Moreover, the drive channels for each qubit are set to their corresponding fitted transition frequencies. As a result, the target qubit undergoes a rotation due to entanglement.

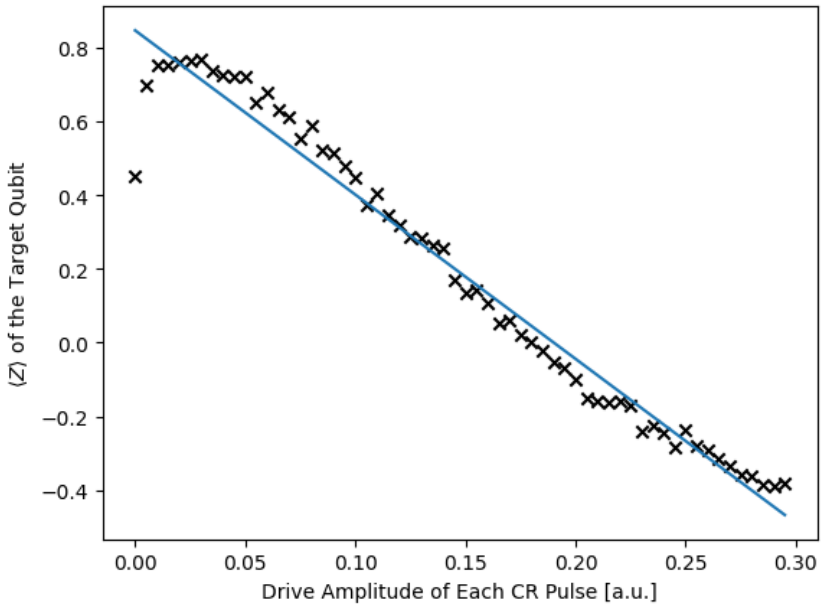

Figure 5: Amplitude Experiment Results. We note that the fit is almost linear as the CR amplitude increases within this range of amplitudes. When the amplitude is less than 0.05, we observe a skew of results relative to the rest of the results, possibly due to a change in frequency on the control channel with a lack of significant drive amplitude causing detuning on the target qubit.

From looking at the IQ Data of the target qubit and applying the classifer, we find that the average expecation is closest to 0 when the amplitude is 0.18. While the fit reports otherwise, one notes that a sanity check of applying the circuit at the fitted amplitude and the approximate amplitude of 0.18 leads to an expectation value discrepancy, and the reported expectations differ by around 0.1 according to the fit results and the raw data. For $A = 0.18$, $\langle Z \rangle_{\text{target}} \approx 0.002$ when considering not considering the measured $|0\rangle$ population and $\langle Z \rangle_{\text{target}} \approx 0.019$ when considering the $|0\rangle$ population. Interestingly this calibrated amplitude is not too far off of the IBM backend amplitude for the $|0\rangle - |1\rangle$ CR gate.

1.1.2 CR Gate Hamiltonian Tomography

Using the calibrated amplitude above, we perform a Hamiltonian Tomography experiment to calculate the CR tones on the control channel. A Hamiltonian Tomography experiment consists of varying the duration τ of the individual pulses on the control channel and subsequently measuring the target qubit in the X, Y, Z Pauli bases. To accomplish the measurements, we construct a hadamard gate by driving a gaussian pulse to our target qubit at $\frac{\text{amp}_\pi}{2}$ drive amplitude for the target qubit. The duration of this gate is the same as the generalized NOT gate.

Since a change one can change bases from the Z basis to the X basis by applying a hadamard, applying a hadamard gate on the target qubit after applying our half-finished CR-gate and measuring in the Z basis gives us the corresponding state in the X basis. This can be observed by the fact that $HZH = X$. Similarly, for the Y basis, after applying the CR gate, we apply the $S^\dagger$ gate and the hadamard gate and measure in the Z basis since $SHZHS^\dagger = Y$. Indeed, by applying these gates, one observes that for an initial state $|\psi\rangle$, $\langle\psi|HZH|\psi\rangle = \langle\psi|X|\psi\rangle = \langle X\rangle$ and $\langle\psi|SHZHS^\dagger|\psi\rangle = \langle\psi|Y|\psi\rangle = \langle Y\rangle$. An example of a tomography circuit is below in Figure 6.

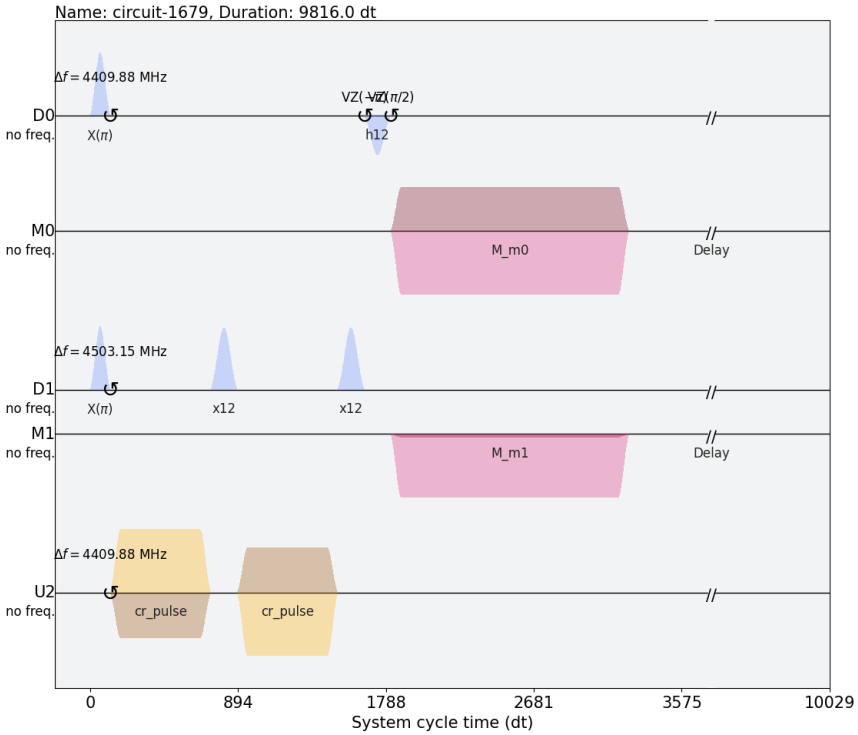

Figure 6: Hamiltonian Tomography Circuit for the CR gate. Here the state is initialized in $|11\rangle$ and is the target qubit is measured in the Y basis as indicated by the rotations. Note that this circuit also includes the calibrated phase on the control channel

As done in [5], we perform a first tomography experiment varying the width of CR pulse on the control channel from $0ns$ and $1600ns (> 5 \times$ normal pulse length) where we sample 21 uniformly distributed times within this interval and average over each circuit 1536 times. We then take the

results and plot the pulse width vs the expectation values of the target qubit with respect to the measured Pauli basis and report the fitted coefficients ω_{ij}. Note that we need to fit each curve simultaneously, so optimization is particularly difficult when the data is far from theoretical expectations. We get the following results for the first tomography experiment: The results from this

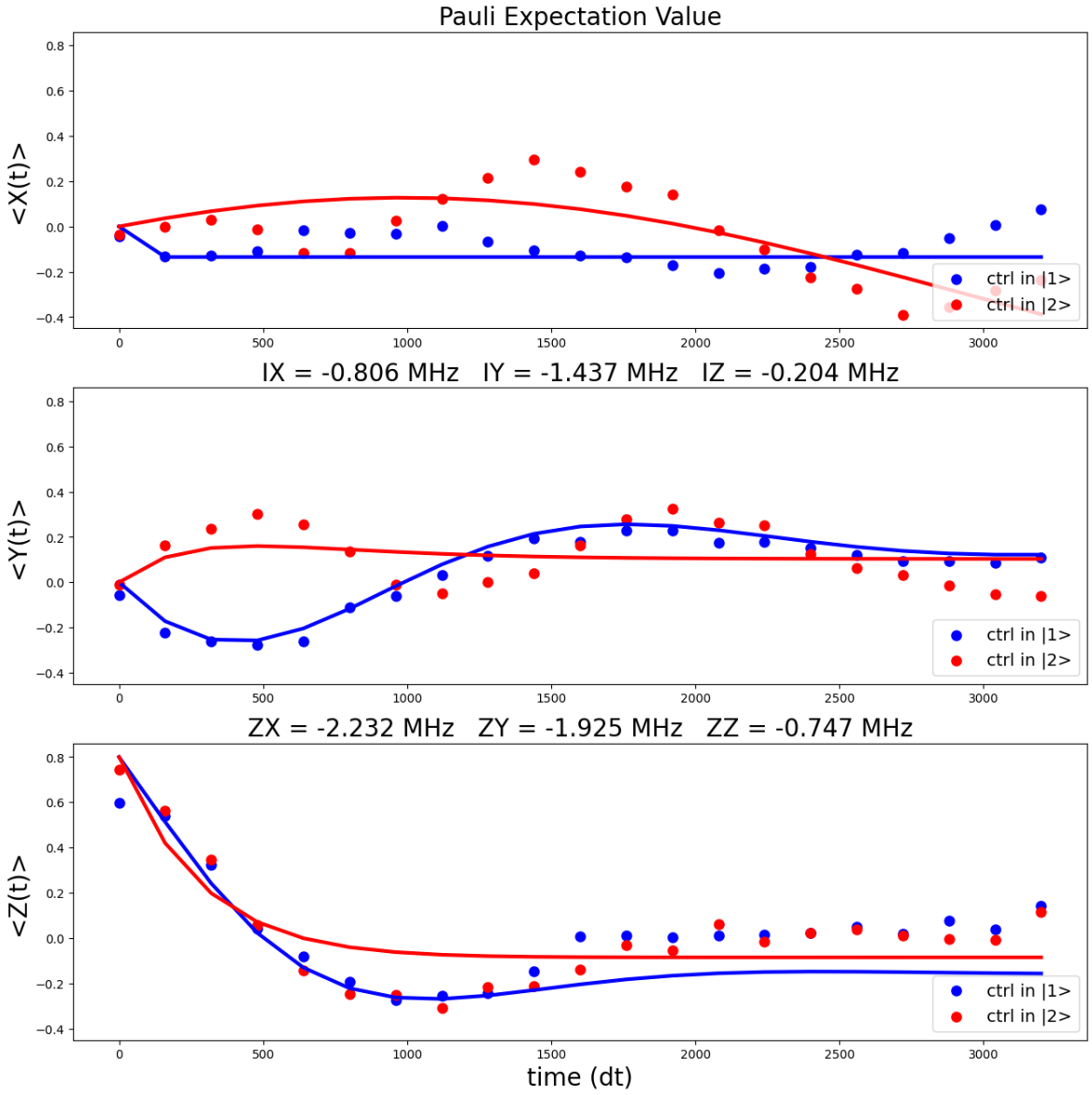

Figure 7: First tomography experiment. We observe clear exponential decay, leading to observed decoherence of the qubits after $\approx 1700dt = 850ns$. To fit the data appropriately to the observed dynamics, we incorporate a damped oscillations fit, adding an extra $e^{-t/T}$ in from of the sinusoidal components of the fit functions. Here, t is the pulse length in ns and T is the decay time. Note that each expectation value appears to have its own decay. For instance, the Z expectation appear to damp heavily after around $850ns$, but the X expectation when the control qubit is $|2\rangle$ doesn't show decoherence. For reference of what ideal CR Tomography looks like, we refer to [5] or the Appendix.

experiment could possibly be related to the discussion in the introduction in that the qubits are resisting rotations that would normally be caused by correlated errors from leakage. Other explanations could be the detuning of the control qubit as the drive duration increases, but data indicates that the Z expectation of the control qubit is relatively the same throughout the experiment, albeit much lower than desired/expected. Nonetheless, from this experiment, we are supposed to gather the phase on the control channel CR pulse to eliminate the ω_{ZY} term in the Hamiltonian. In particular, the CR phase is $\phi_0 = -\tan^{-}(\omega_{ZY}/\omega_{ZX})$. Unfortunately, due to the inability to properly fit data and possible other dynamics, this phase is actually ineffective upon testing more iterations of the tomography experiment, but after performing the tomography and re-calibrating the phase multiple times, we find $\phi_0 \approx 5.66$ radians.

Normally, one would conduct more tomography experiments to calibrate the amplitude of the cancellation rotations on the target qubit to reduce ω_{IX} and ω_{IY} as seen in Figures 2 and 3, but we stop here since we don't have a proper calibration to know where errors in experiments are coming from.

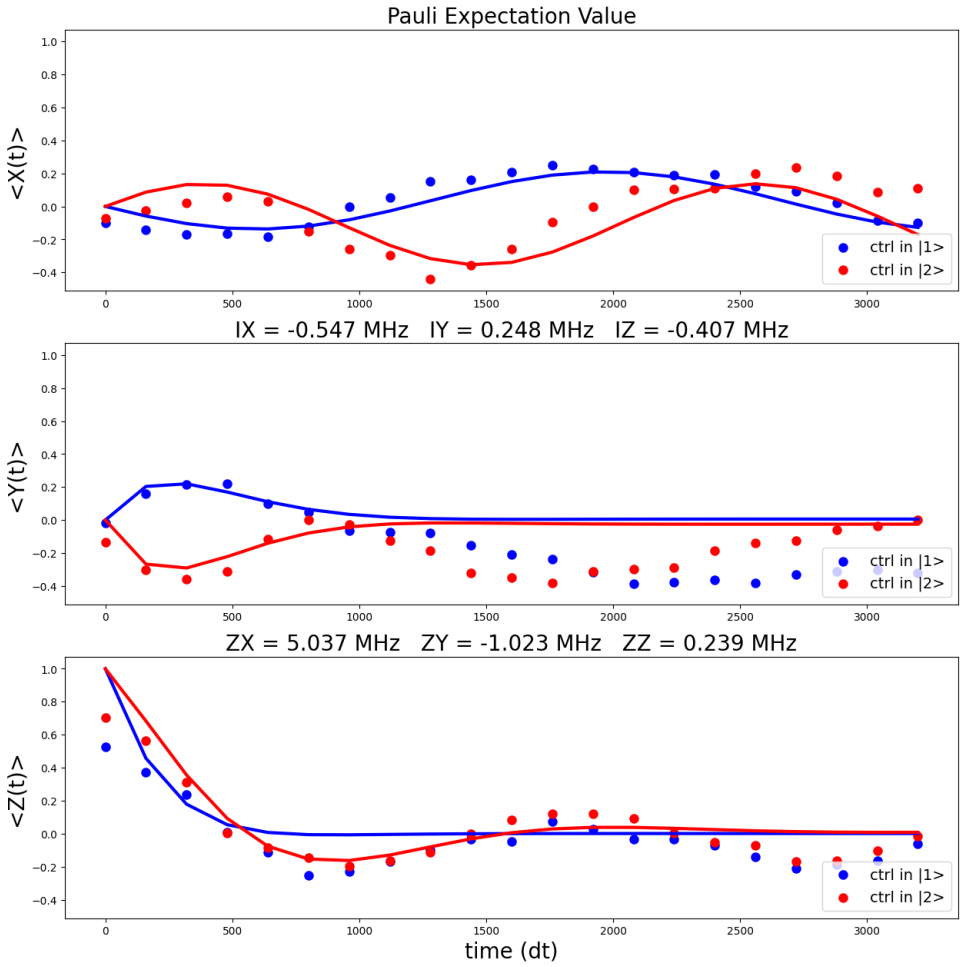

Figure 8: Hamiltonian Tomography of the CR gate for a relatively properly calibrated phase ϕ_0. While possibly due to poor fitting of $\langle Y(t)\rangle$, we observe a higher ω_{ZX} coefficient, which is a step in the right direction since maximizing this term means the gate is performing well. Moreover, we also observe less decay of $\langle Z(t)\rangle$, which indicates that the phase helped improve the gate. Error Thresholds for the Interactions rates are as follows: ± 0.282, ± 0.0659, ± 0.295, ± -0.018, ± 0.169, and ± 0.0026 for $\omega_{ZX}, \omega_{IX}, \omega_{ZY}, \omega_{IY}, \omega_{ZZ}, \omega_{IZ}$ respectively. All units of the error thresholds are MHz.

1.2 Quantum State Tomography

Now, to answer the question: Given these difficulties in the calibration process, how accurate are states output by this gate? Quantum State Tomography (QST) is the process of performing measurements with respect to an operator basis $\{E_i\}_{i=1}^{d^2}$ to reconstruct the density matrix of a state as it undergoes a transformation by a gate. We denote the quantum channel that implements the CR gate by $\mathcal{E}_{CR}$. After initializing a state ρ, we perform $\mathcal{E}_{CR}(\rho)$ and measure in the different pairs of Pauli Bases $XX, XY, XZ, YX, YY, YZ, ZX, ZY, ZZ$ where the $\otimes$ is removed for readability. After performing these measurements, we define our operator basis $\{\sigma_0\sigma_1\}_{\sigma_1,\sigma_2\in\{I,X,Y,Z\}}$ and calculate $\langle\sigma_0\sigma_1\rangle = Tr(\sigma_0\sigma_1\rho)$. Here, the subscripts represent the qubit that is being acted on. After finding

these expectation values, the experimental density matrix that we reconstructed is then

$$\rho_{\text{exp}} = \frac{1}{4} \sum_{\sigma_0,\sigma_1 \in \{I,X,Y,Z\}} Tr(\sigma_0 \sigma_1 \rho_{\text{ideal}}) \sigma_0 \sigma_1$$

We execute the 9 QST circuits and average over 4096+ shots per circuit, providing extremely accurate data. Out of this data, around 4% demonstrated leakage into the $|0\rangle$ (for both the control and the target qubit). After reconstructing density matrix ρ_{exp} from the measurement data, we compute the fidelity between the experimental density matrix and the ideal density matrix via

$$F(\rho_{\text{ideal}}, \rho_{\text{exp}}) = (Tr(\sqrt{\sqrt{\rho_{\text{ideal}}} \rho_{\text{exp}} \sqrt{\rho_{\text{ideal}}}})^2$$

Note that the theoretical density matrices are

$$\rho_{11} = \rho_{21} = \begin{pmatrix} 0.5 & 0 & 0 & 0 \\ 0 & 0 & 0 & 0 \\ 0 & 0 & 0.5 & 0 \\ 0 & 0 & 0 & 0 \end{pmatrix} \qquad \rho_{22} = \rho_{12} = \begin{pmatrix} 0 & 0 & 0 & 0 \\ 0 & 0.5 & 0 & 0 \\ 0 & 0 & 0 & 0 \\ 0 & 0 & 0 & 0.5 \end{pmatrix} \tag{1.4}$$

When we initialize in the $\{|1\rangle, |2\rangle\}$ computational basis states, we found the following heatmaps of entries.

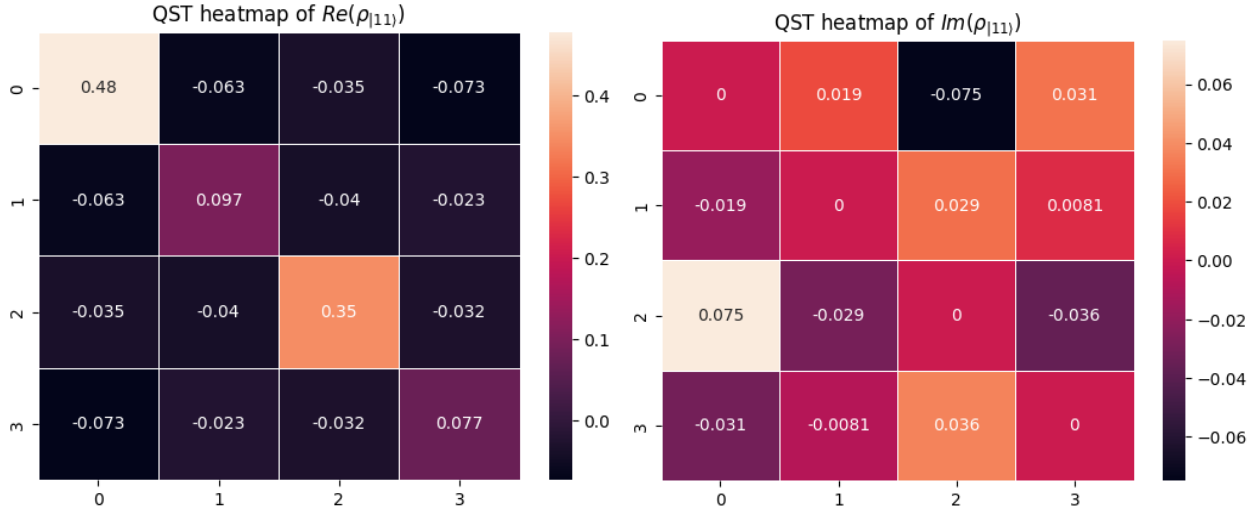

(a) Real component of QST-constructed density matrix for initial state $|11\rangle$

(b) Imaginary component of QST-constructed density matrix with initial state $|11\rangle$

Figure 9: QST Heatmaps for Experimental Density Matrices for the $|11\rangle$ computational basis state where the indices on the x and y axes correspond to matrix indices. For a key, $|11\rangle \leftrightarrow (0,0)$, $|12\rangle \leftrightarrow (1,1)$, $|21\rangle \leftrightarrow (2,2)$, $|22\rangle \leftrightarrow (3,3)$. The correspondence of other entries can be deduced from these four indications. We find a state fidelity of 82.035%.

Interestingly, for initial states not equal to $|11\rangle$, the reconstructed density matrix indicates that the

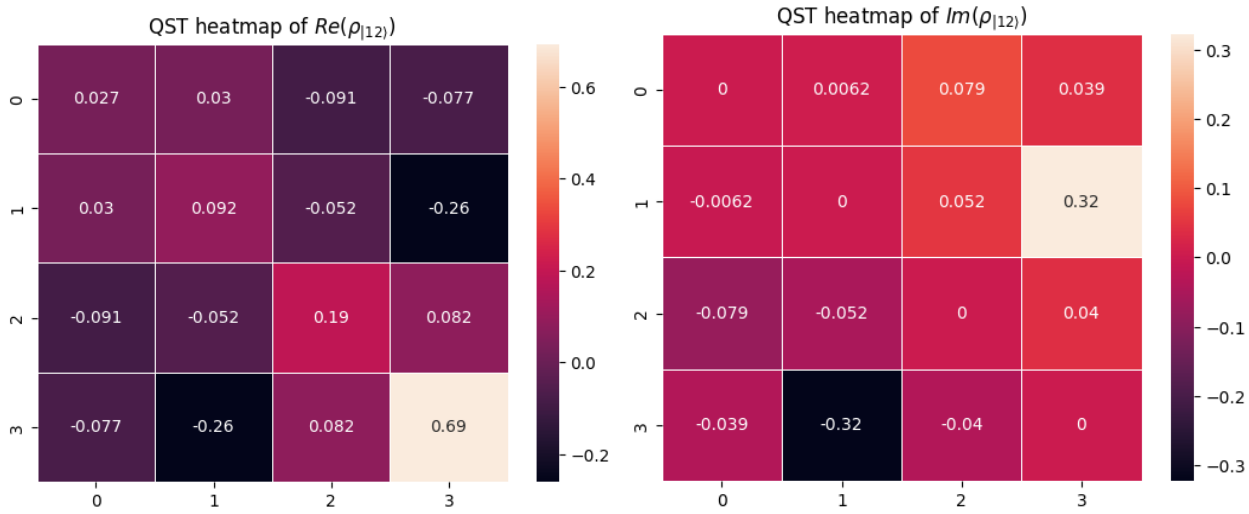

(a) Real component of QST-constructed density matrix for initial state $|12\rangle$

(b) Imaginary component of QST-constructed density matrix with initial state $|12\rangle$

Figure 10: QST Heatmaps for Experimental Density Matrices for the $|12\rangle$ computational basis state. We find a state fidelity of 64.589%.

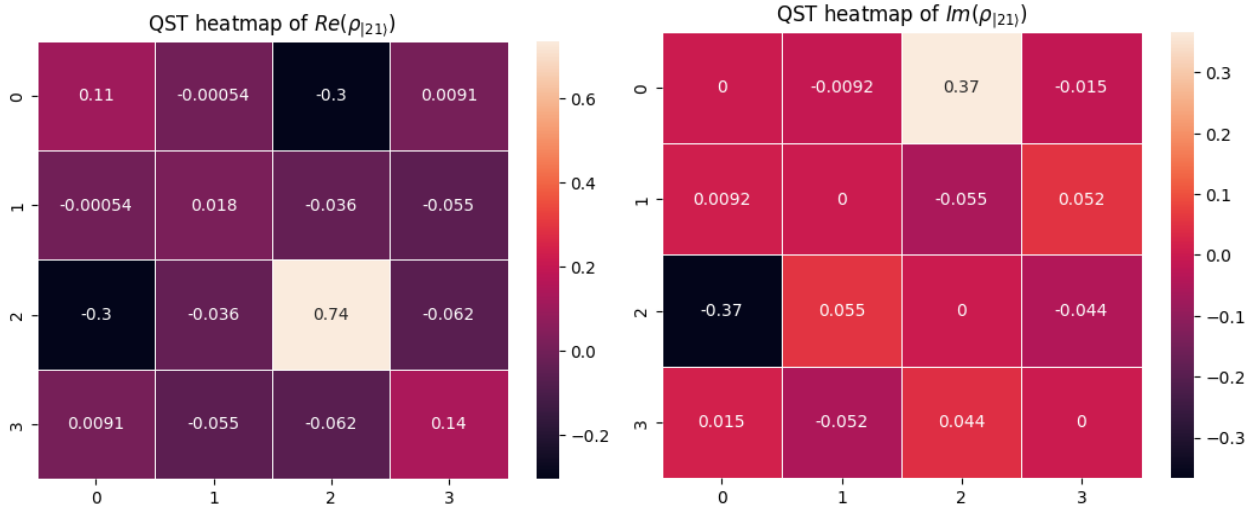

(a) Real component of QST-constructed density matrix for initial state $|21\rangle$

(b) Imaginary component of QST-constructed density matrix with initial state $|21\rangle$

Figure 11: QST Heatmaps for Experimental Density Matrices for the $|21\rangle$ computational basis state. We find a state fidelity of 70.86%.

state did not want to deviate from the initial state particularly much under the CR gate. Moreover, there are very nonneglible imaginary components to the reconstructed matrix, indicating that there is still a nonnegligible Y component to the gate (Y is the only Pauli with imaginary entries).

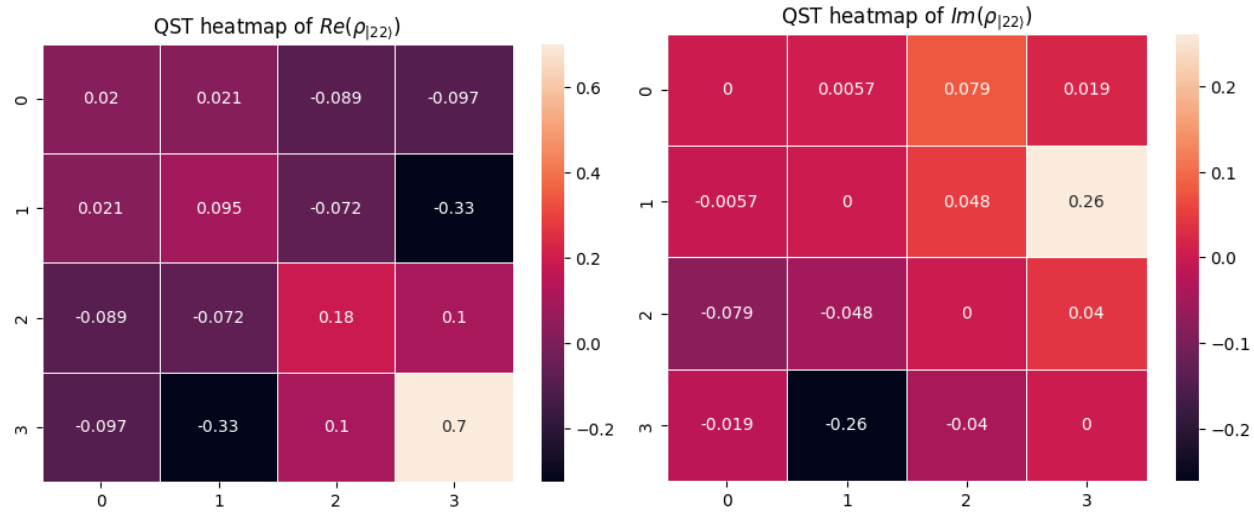

(a) Real component of QST-constructed density matrix for initial state $|22\rangle$

(b) Imaginary component of QST-constructed density matrix with initial state $|22\rangle$

Figure 12: QST Heatmaps for Experimental Density Matrices for the $|22\rangle$ computational basis state. We find a state fidelity of 65.64%.

2 Conclusion

The goal of this experiment was to calibrate a Cross Resonance Gate between the $|1\rangle$ and $|2\rangle$ states. While we achieved partial calibration by performing amplitude sweeps of the pulses on the control channel and hamiltonian tomography experiments, the latter experiments began showing the larger deviations from theoretical outcomes. In particular, instead of displaying CR Rabi Oscillations for Pauli time-dependent Expectations as CR pulse width increased, these time dependent expectations underwent some sort of damping as pulse width increased. Moreover, each expectation value had its own decay time, with $\langle Z\rangle$ having the most prevalent decay.

After calibrating the phase of the CR pulse, we perform Quantum State Tomography to observe where possible errors and how this somewhat calibrated gate acts on the computational basis $\{|11\rangle, |12\rangle, |21\rangle, |22\rangle\}$. The most prominent and unexpected result was an $\approx 82\%$ state fidelity when the $|11\rangle$ state is passed through our CR gate, but other basis states acted as expected with $\leq 70\%$ state fidelities.

Quantum Process Tomography would provide a better description of the gate since it would allow us to calculate gate fidelity, so this is something to look to in the future. Moreover, since difficulties in this experiemnt were likely encountered due to resilience of quantum computers against leakage into the $|2\rangle$ state, it would be nice to have the opportunity to work with the hardware of a transmon computer to bypass these safeguards and observe the dynamics of Cross Resonance on higher energy states. More importantly, it would confirm what exactly is going wrong within these experiments. Are the dynamics of the $|2\rangle$ simply that bad? Or is it something deeper in the hardware. I'm inclined to believe both equally due to past work utilizing the $|2\rangle$ in

experiments as discussed in the introduction, but what exactly allows the $|2\rangle$ to function in those settings rather than this one? Nonetheless, these are questions and avenues to pursue in the future.

3 Appendix

3.1 Basic Gate Calibrations

3.1.1 Transition Frequencies

To determine the transition frequencies of $|1\rangle \rightarrow |2\rangle$ of each qubit, we gain a rough estimate of the transition frequency via (its frequency) − (its anharmonicity) and perform pulse sweeps for 75 uniformly distributed points in a radius of 30MHz around this estimated frequency. We fit the resulting data to a Lorentzian curve and acquire the transition frequency from the fitted center of the curve. We find the fitted transition frequencies to be: $4.50 \pm 0.00025 GHz$ and $4.409881 \pm 0.0002 GHz$ for qubits 1 and 0 respectively.

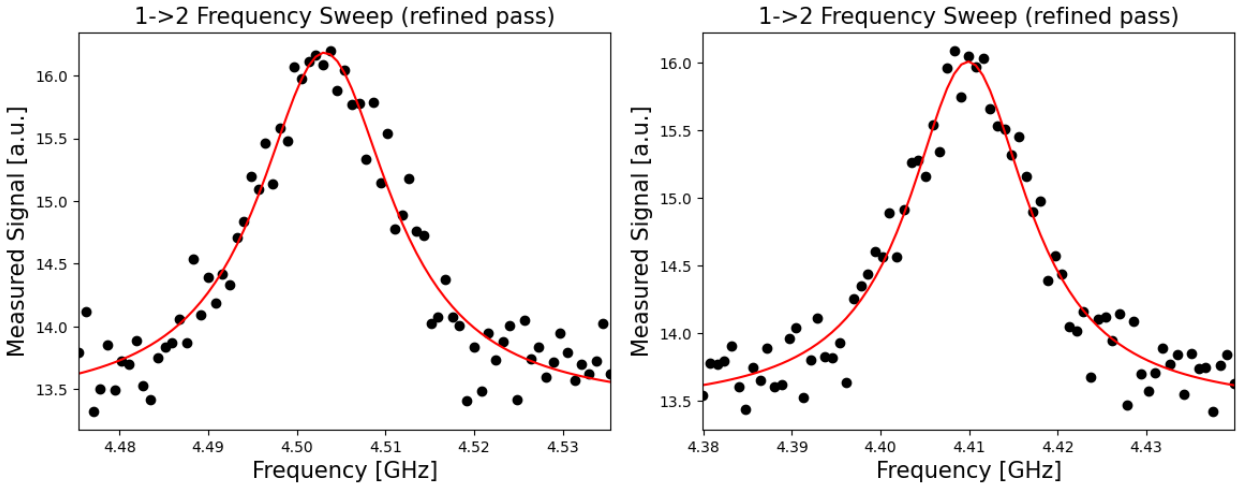

(a) $|1\rangle \rightarrow |2\rangle$ Frequency Sweep for Qubit 1

(b) $|1\rangle \rightarrow |2\rangle$ Frequency Sweep for Qubit 0

Figure 13: Transition Frequency Sweeps

3.1.2 π-pulse amplitudes

Using the transition frequencies we found in the first experiment, we do an amplitude sweep, sweeping 75 uniformly distributed amplitudes in $[0, 1] \subset \mathbb{R}$ and applying gaussian pulses at these varied amplitudes and the calibrated transition frequency, thus inducing Rabi oscillations on the qubits. We fit these oscillations to a sinusoidal curve and extract the drive period T, and the proper amplitude will be $T/2$. We find the $\pi-$pulse amplitudes to be 0.184 ± 0.0016 and 0.245 ± 0.0038 for qubits 1 and 0 respectively. Now that we have a calibrated X gate from these two experiments, we build a classifier to perform classical measurements in future experiments. We do this by performing

operations to inject the $|0\rangle, |1\rangle, |2\rangle$ state into the qubit and performing each circuit for 2048 shots. We feed this data along with expected values into a classical *Support Vector Machine* which will become our classifier for future experiments.

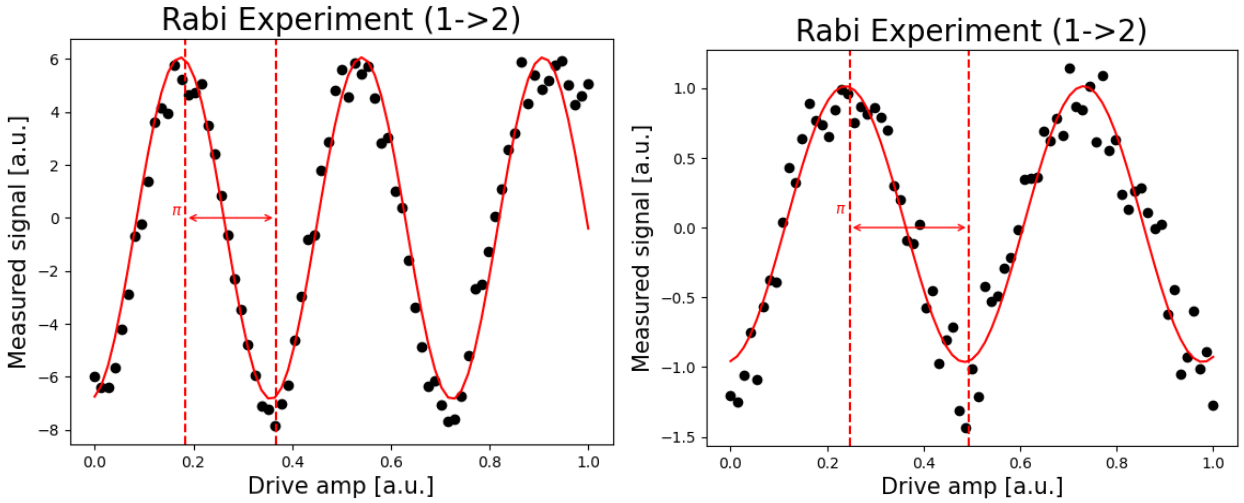

(a) Rabi Experiment for Qubit 1

(b) Rabi Experiment for Qubit 0

Figure 14: π pulse amplitude sweeps

3.1.3 Hamiltonian Tomography Fit Functions

"In order to extract the coefficients ω_{ij}, we look at the expectation value of Pauli operators as a function of pulse duration. Since the evolution of the expectation value of an operator $\hat{O}$ can be given as:

$$\langle \hat{O}(t) \rangle = \langle e^{i\hat{H}t} \hat{O} e^{-i\hat{H}t} \rangle$$

where $\hat{H}$ is the hamiltonian for our gate, for an infinitesimally small time increment dt, we have:

$$\langle \hat{O}(t+dt) \rangle = \langle (1 + i\hat{H}dt)\hat{O}(t)(1 - i\hat{H}dt) \rangle = \langle \hat{O}(t) \rangle + idt \langle \left[\hat{H}, \hat{O}\right] \rangle \implies \frac{d\langle \hat{O} \rangle}{dt} = i \left[\hat{H}, \hat{O}\right]$$

to first order in dt. We can evaluate the commutator for each of the Pauli operators on the target qubit:

$$\left[\hat{H}, \hat{I}\hat{X}\right] = 2i \left(a_y \hat{Z}\hat{Z} - a_z \hat{Z}\hat{Y} + b_y \hat{I}\hat{Z} - b_z \hat{I}\hat{Y}\right)$$

$$\left[\hat{H}, \hat{I}\hat{Y}\right] = 2i \left(-a_x \hat{Z}\hat{Z} + a_z \hat{Z}\hat{X} - b_x \hat{I}\hat{Z} + b_z \hat{I}\hat{X}\right)$$

$$\left[\hat{H}, \hat{I}\hat{Z}\right] = 2i \left(a_x \hat{Z}\hat{Y} - a_y \hat{Z}\hat{X} + b_x \hat{I}\hat{Y} - b_y \hat{I}\hat{X}\right)$$

If we let n be the expectation value of the Pauli $\hat{Z}$ operator on the control qubit, then we can write down these commutators in terms of the expectation values of the target qubit:

$$i\langle\left[\hat{H},\hat{I}\hat{X}\right]\rangle_{\text{control}} = 2\left(na_z + b_z\right)\langle\hat{Y}\rangle - 2\left(na_y + b_y\right)\langle\hat{Z}\rangle$$

$$i\langle\left[\hat{H},\hat{I}\hat{Y}\right]\rangle_{\text{control}} = 2\left(na_x + b_x\right)\langle\hat{Z}\rangle - 2\left(na_z + b_z\right)\langle\hat{X}\rangle$$

$$i\langle\left[\hat{H},\hat{I}\hat{Z}\right]\rangle_{\text{control}} = 2\left(na_y + b_y\right)\langle\hat{X}\rangle - 2\left(na_x + b_x\right)\langle\hat{Y}\rangle$$

where the expectation values on the right hand side are those of the target qubit. Define $\vec{r_n} = \{\langle\hat{X}\rangle, \langle\hat{Y}\rangle, \langle\hat{Z}\rangle\}_n$, so we can use the above commutators to write down a matrix equation $\frac{d}{dt}\vec{r(t)}$ depending on n. This yields:

$$\frac{d}{dt}\begin{bmatrix}\langle\hat{X}\rangle\\ \langle\hat{Y}\rangle\\ \langle\hat{Z}\rangle\end{bmatrix} = 2\begin{bmatrix}0 & na_z + b_z & -na_y - b_y\\ -na_z - b_z & 0 & na_x + b_x\\ na_y + b_y & -na_x - b_x & 0\end{bmatrix}\begin{bmatrix}\langle\hat{X}\rangle\\ \langle\hat{Y}\rangle\\ \langle\hat{Z}\rangle\end{bmatrix} \tag{3.1}$$

$$\frac{d\vec{r}_n(t)}{dt} = G_n\vec{r}_n(t) \tag{3.2}$$

where

$$G_n = 2\begin{bmatrix}0 & na_z + b_z & -na_y - b_y\\ -na_z - b_z & 0 & na_x + b_x\\ na_y + b_y & -na_x - b_x & 0\end{bmatrix} \equiv \begin{bmatrix}0 & \Delta^n & -\Omega_y^n\\ -\Delta^n & 0 & \Omega_x^n\\ \Omega_y^n & -\Omega_x^n & 0\end{bmatrix}.$$

Since G_n is time independent, integrating the differential equation with the initial state at $t = 0$, we have

$$\vec{r}_n(t) = e^{G_n t}\vec{r}_n(0).$$

We can find the matrix exponential, $e^{G_n t}$, by finding the eigenvalues and eigenvectors of G_n. The eigenvalues of G_n are

$$\vec{g}_n = \{0, -i\sqrt{\Delta^2 + \Omega_x^2 + \Omega_y^2}, i\sqrt{\Delta^2 + \Omega_x^2 + \Omega_y^2}\}_n,$$

where the subscript n represents the state of the control qubit from which we get $\Delta, \Omega_x, \Omega_y$. Let U be the eigenbasis transformation and let $\hat{D}_n$ be the diagonal matrix of the eigenvalues. Then we can rewrite $\vec{r}_n(t)$ as

$$\vec{r}_n(t) = U^\dagger e^{\hat{D}_n t} U\vec{r}_n(0).$$

Setting $\vec{r}_n(0) = \{0, 0, 1\}$ (which corresponds the target qubit starting in the $|1\rangle$ state) we have that

$$\langle\hat{X}(t)\rangle_n = \frac{1}{\Omega^2}\left(-\Delta\Omega_x + \Delta\Omega_x\cos(\Omega t) + \Omega\Omega_y\sin(\Omega t)\right)$$

$$\langle \hat{Y}(t) \rangle_n = \frac{1}{\Omega^2} \left(\Delta\Omega_y - \Delta\Omega_y \cos(\Omega t) - \Omega\Omega_x \sin(\Omega t) \right)$$

$$\langle \hat{Z}(t) \rangle_n = \frac{1}{\Omega^2} \left(\Delta^2 + \left(\Omega_x^2 + \Omega_y^2 \right) \cos(\Omega t) \right)$$

where $\Omega = \sqrt{\Delta^2 + \Omega_x^2 + \Omega_y^2}$ for each control qubit preparation n." [6]

3.2 CR Gate Hamiltonian Tomography on the standard $\{|0\rangle, |1\rangle\}$ basis

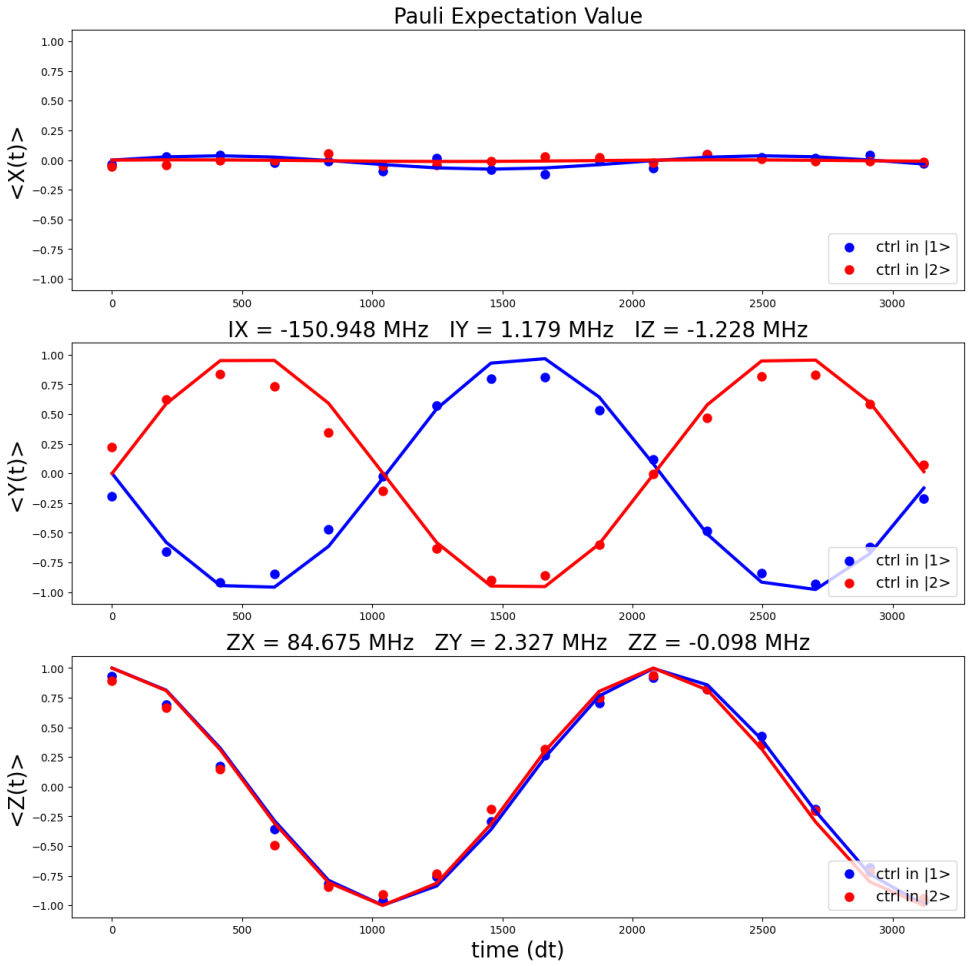

Figure 15: Fully Calibrated CR gate Hamiltonian Tomography on $\{|0\rangle, |1\rangle\}$. Notice the extremely large ZX interaction rate while other interaction rates aside from IX are relatively small. Compared to the excited energy level case, the expectation values reach peak saturations of 1 and -1.

References

[1] Miao, K.C., McEwen, M., Atalaya, J. et al. Overcoming leakage in quantum error correction. Nat. Phys. 19, 1780–1786 (2023). https://doi.org/10.1038/s41567-023-02226-w.

[2] Galda, A. Cubeddu, M., Kanazawa, N. et al. Implementing a Ternary Decomposition of the Toffoli Gate on Fixed-Frequency Transmon Qutrits. `https://arxiv.org/pdf/2109.00558`

[3] Di, Y. and Wei, H. Elementary gates of ternary quantum logic circuit. `https://arxiv.org/pdf/1105.5485.pdf`

[4] Thomas Alexander et al. 2020 *Quantum Sci. Technol.* 5 044006.

[5] Danin, D. and Tennie. F. Procedure for improving cross-resonance noise resistance using pulse-level control. `https://arxiv.org/pdf/2303.12771.pdf`

[6] The Qiskit Team, "Hamiltonian Tomography," `https://qiskit.org/textbook/ch-quantum-hardware/hamiltonian-tomography.html` (2022).